Electronic Supplementary Material (ESI) for Physical Chemistry Chemical Physics.

Supplementary Material

High Resolution Absolute Absorption Cross Sections of the $\tilde{B}^1A'$–$\tilde{X}^1A'$ Transition of the CH_2OO Biradical

Elizabeth S. Foreman,[1] Kara M. Kapnas,[1] YiTien Jou,[1] Jarosław Kalinowski,[2] David Feng,[3] R. Benny Gerber,[1,2,4,a] and Craig Murray[1,b]

1. *Department of Chemistry, University of California, Irvine, Irvine CA 92697, USA*
2. *Department of Chemistry, A.I. Virtasen aukio 1 (P.O. BOX 55) FI-00014, University of Helsinki, Finland*
3. *Department of Mechanical and Aerospace Engineering, University of California, Irvine, Irvine CA 92697, USA*
4. *Institute of Chemistry, Hebrew University, Jerusalem 91904, Israel*

[a] Email: benny@fh.huji.ac.il, Telephone: +972-2-651-3742

[b] Email: craig.murray@uci.edu; Telephone: +1-949-824-4218

Collinear Photolysis Cavity Ring-Down Spectroscopy

The layout of the collinear and counter-propagating photolysis-probe cavity ring-down (CRD) spectrometer is illustrated in Figure S1.

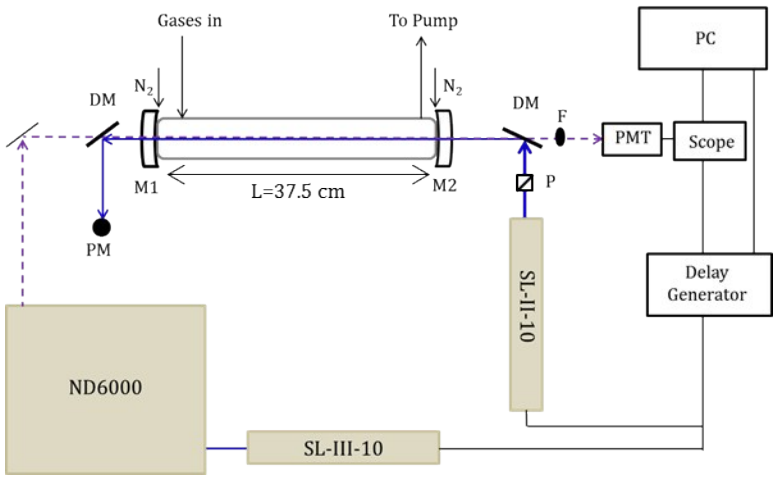

Figure S1: CRDS experimental schematic. (PM=power meter, DM=dichroic mirror, M1 and M2=highly reflective CRD mirrors, F=dichroic filter, P=polarizer, PMT=photomultiplier tube, dashed purple=probe beam, solid blue=photolysis beam).

The 355 nm photolysis beam is steered into the flow cell through the rear cavity mirror (M2) using a 355 nm Razor Edge long-pass dichroic mirror (Semrock) that reflects only the 355 nm beam while transmitting the longer wavelength probe radiation through the filter to the PMT. An identical dichroic placed before the front cavity mirror (M1) directs the transmitted 355 nm radiation to a beam dump or energy meter. The photolysis pulse energy is measured using an energy meter at three locations: before M1, after transmission through M1 only, and after transmission through both M1 and M2. Although the CRD mirrors are only *highly* reflective over the 415–465 nm range, the 355 nm back reflection from M2 is ~50% of the incident energy. During data acquisition the power of the photolysis laser is continuously measured after exiting the cavity.

In order to prevent damage to the ring-down mirrors, the low photolysis pulse energies were used. Peak-to-peak stability of 12% with a pulse energy of <5 mJ was achieved by operating the photolysis laser at the optimum Q-switch delay and variably attenuating the beam with a polarizer. These conditions are well below the damage threshold for the ring-down mirrors at 355 nm (20 W cm^{-2}).

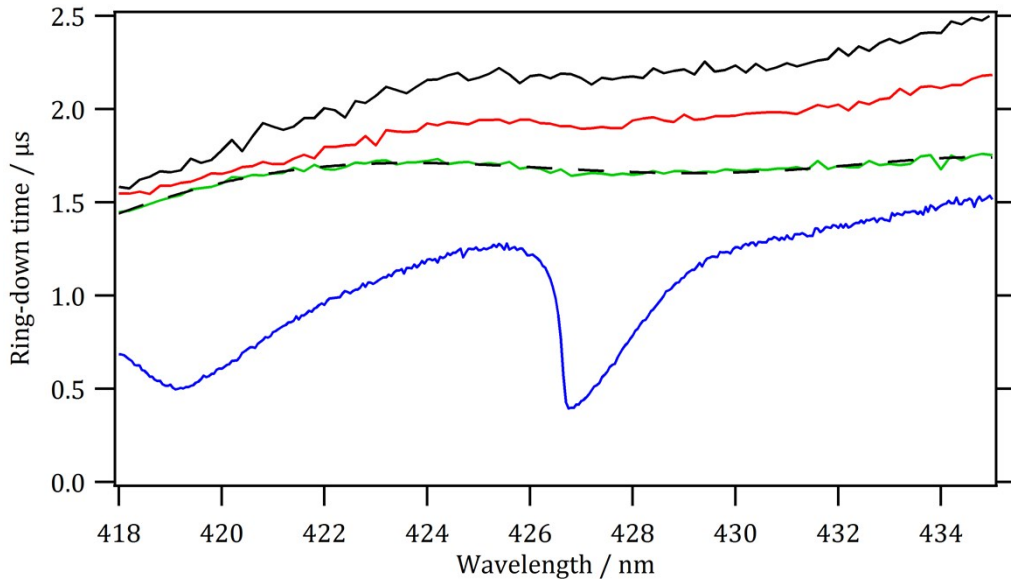

Figure S2: Raw ring-down time as a function of wavelength: black = gas off, photolysis off; red=gas off, photolysis on at Δt =180 ms; green = gas on and photolysis on at Δt = 180 ms; blue = gas on and photolysis on at Δt = 140 µs showing IO absorption. The black dashed line represents high order polynomial fit, $\tau_{0,fit}(\lambda)$, to the empty cavity ring-down, $\tau_0(\lambda)$.

The effects of the incident photolysis beam on the performance of the optical cavity have been examined. A modest (~2–12%), wavelength-dependent decrease in ring-down time was observed to occur over a timescale of ~ 2 s after exposure to the photolysis beam, after which it remained stable (see Figure S2). Nevertheless the photolysis and probe beams were allowed to pass through the ring-down mirrors for several minutes before commencing data collection as a precaution,. No long term decrease in the ring-down time due to the photolysis laser was

observed. The standard deviations in the fitted ring-down times did not increase upon exposure to the photolysis beam. Larger reductions of 37−50% have been reported in other collinear photolysis cavity ring-down experiments.[1,2] It may be that the dielectric coatings of the ring-down mirrors are less sensitive to local heating effects induced by the photolysis beam.

The empty cavity ring-down time, $\tau_0(\lambda)$, was measured as a function of probe laser wavelength with and without the incident photolysis beam, and is shown in Figure S3. $\tau_0(\lambda)$ was measured with relatively large wavelength step sizes (0.2 nm step) and fit to a high order polynomial, which was used to calculate $\alpha(\lambda)$. High resolution scans over narrower spectral windows found no reproducible structure in $\tau_0(\lambda)$ either with or without the photolysis beam present.

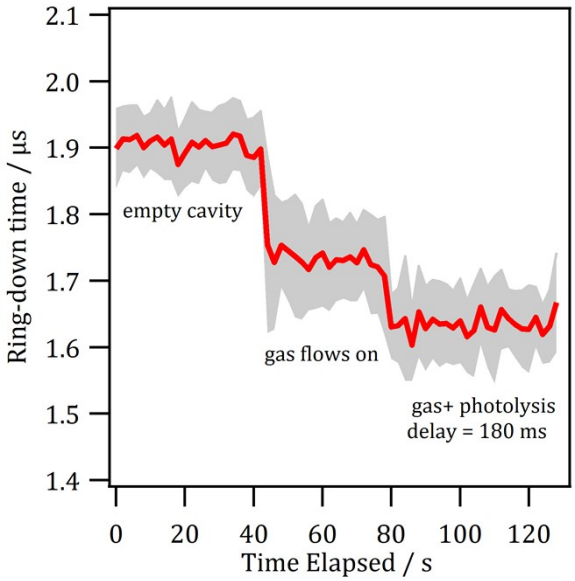

Figure S3: Perturbation to the ring-down time by addition of gas mix (0.03% CH_2I_2, 5.4% O_2 and N_2) to the reaction cell and the photolysis beam entering the cavity. Probe wavelength = 427.062 nm. Grey shading represents 1σ uncertainty in the ring-down time. 20 laser shots are averaged per point at 10 Hz.

IO Kinetics

In order to verify the total removal of IO within the period of our measurement, we collected the time profile of IO by probing the $A^2\Pi_{3/2}$–$X^2\Pi_{3/2}$ (4,0) bandhead at 437.062 nm as a function of photolysis-probe time delay (see Figure S4). The ring-down time of <2 μs is sufficiently short relative to the timescale of the process that the IO concentration is effectively constant during the timescale of the ring-down measurement. With the low IO number densities present in these experiments, IO is removed slowly by self-reaction on a timescale of ~90 ms. This is very close to the 100 ms period of a 10 Hz measurement. All spectra were collected at a reduced repetition rate of 5 Hz to avoid IO build-up in the reaction cell.

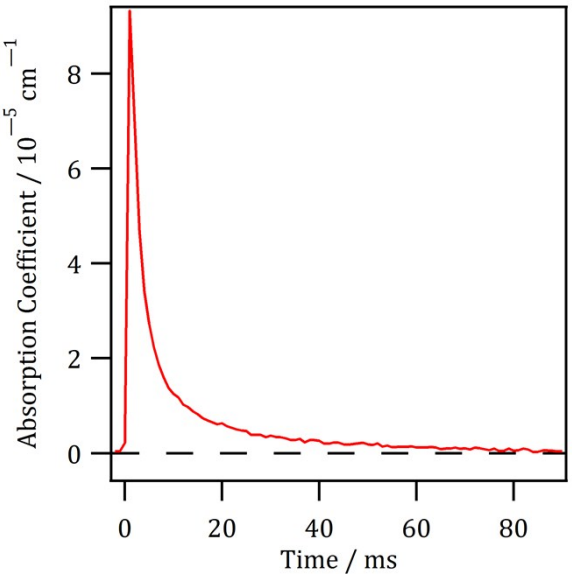

Figure S4: Time profile for IO measured at $A^2\Pi_{3/2}$–$X^2\Pi_{3/2}$ (4,0) bandhead. Probe wavelength = 427.062 nm. Time step = 1 ms.

Determination of Absolute Absorption Cross Sections

Absolute absorption cross sections for CH_2OO are determined by estimating the peak number density present in the flow cell. Two methods were considered for determining the peak CH_2OO number density. The first estimates the initial number density of CH_2I and uses previous measurements of the pressure-dependent CH_2OO yield of the $CH_2I + O_2$ reaction. The initial

CH_2I_2 number density is measured directly by single pass broadband absorption spectroscopy using a UV LED between 350 385 nm and previously reported absorption cross sections.[3] The yield of CH_2I from photolysis, Φ_{CH_2I}, is estimated for a given laser fluence using a value of 1.92×10^{-19} cm^2 for the absorption cross section of CH_2I_2 at 355 nm.[3] The yield of CH_2OO in the $CH_2I + O_2$ reaction, y_{CH_2OO}, is pressure dependent but can be estimated by applying the following expression from Ting *et al*.,[4] to our experimental conditions:

$$y^{-1} = (1.24\pm0.03) + (9.13\pm0.33)\times10^{-20}[\mathrm{M}]$$

where [M] is the total number density. CH_2OO yields determined by other indirect approaches also agree within their mutual uncertainties .[5,6] We have included an additional factor, κ, to correct for the fact that peak CH_2OO number density will be less than the maximum predicted from the total yield. The formation rate, while rapid, is not infinitely fast with respect to the loss rate. We determined phenomenological rates for formation and loss of 3×10^5 s^{-1} and 1.6×10^4 s^{-1} by fitting a kinetic model to a difference of exponentials (see Figure S5). The peak observed number density is only 80.2% of that predicted from the total yield based on our estimates of the formation and loss rates. A summary of the key quantities for both BBTA and CRDS experiments can be found in Table S1. The resulting peak CH_2OO number densities for the broadband and CRDS experiments of $(1.4\pm0.39)\times10^{13}$ cm^{-3} and $(5.1\pm1.4)\times10^{12}$ cm^{-3}, respectively, are calculated using:

$$n_{CH_2OO} = n_{CH_2I_2}\Phi_{CH_2I}y_{CH_2OO}\kappa$$

The relative uncertainties in the estimated CH_2OO number densities of 27% and 28% are the primary sources of error in the absolute absorption cross section.

Table S1: Key Quantities Used in Determination of Absorption Cross Section

	$n_{CH_2I_2}$ / 10^{15} cm^{-3}	Φ_{CH_2I}	y_{CH_2OO}	κ	n_{CH_2OO} / 10^{12} cm^{-3}
BBTA	2.2 ± 0.4	0.011±0.002	0.72 ± 0.05	0.802	14 ± 3.9
CRDS	7.4 ± 1.5	0.0013±0.0002	0.69 ± 0.05	0.802	5.1 ± 1.4

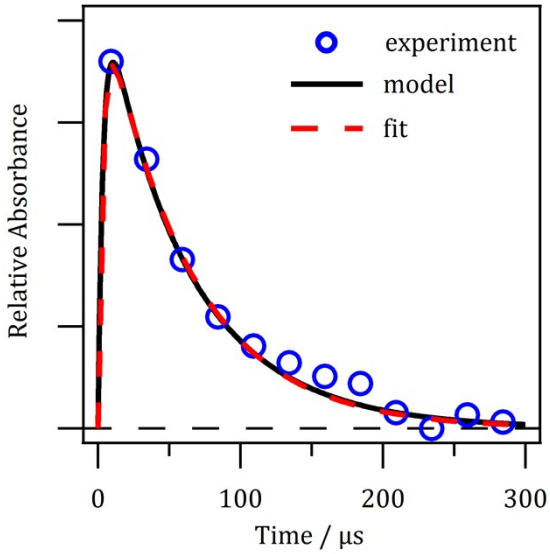

Figure S5: The time profile for CH_2OO measured using broadband transient absorption is shown in blue circles. A kinetic model is shown in solid black, and a fit to the kinetic model is shown in dashed red.

An additional source of error in the CH_2OO number density calculation could be that the number density is not constant over the duration of the 6 μs LED pulse. However our kinetic model predicts that between 10–16 μs, the absorption of CH_2OO varies by only 5%, and has been neglected.

We also considered a second approach exploiting the well-characterized absorption cross sections of IO and relating its number density to that of CH_2OO. The very different temporal behavior requires the use of a kinetic model to account for the time-dependence of both species. This approach is complicated by the uncertainty in the time-dependent relative yields of IO and CH_2OO. The absorption cross sections for the A–X band of IO are well known and the number

density of IO can be readily measured.[7,8] Estimating the yield of IO relative to CH_2OO, however, is less straightforward. IO is produced both directly and from secondary chemistry,[9] and the pressure-dependence is not well characterized. Particularly, the early time behavior is determined by the fraction of the $CH_2I + O_2$ reaction that produces IO directly. In previous work, we have shown that this fraction is likely dependent upon the degree of initial excitation of the photolytically-generated reactant CH_2I.[9] The CH_2I^* collisional relaxation rate in an N_2/O_2 bath has not been quantified experimentally, which obscures the branching fraction. This process will be the subject of a following publication. Until then, we are not confident that we can reliably estimate the relative time-dependent IO and CH_2OO number densities.

References

1 K. J. Feierabend, J. E. Flad, S. S. Brown and J. B. Burkholder, *J. Phys. Chem. A*, 2009, **113**, 7784–7794.
2 J. E. Flad, S. S. Brown, J. B. Burkholder, H. Stark and A. R. Ravishankara, *Phys. Chem. Chem. Phys.*, 2006, **8**, 3636–3642.
3 Sander, S. P., J. Abbatt, J. R. Barker, J. B. Burkholder, R. R. Friedl, D. M. Golden, R. E. Huie, C. E. Kolb, M. J. Kurylo, G. K. Moortgat, V. L. Orkin and P. H. Wine, 2011.
4 W.-L. Ting, C.-H. Chang, Y.-F. Lee, H. Matsui, Y.-P. Lee and J. J.-M. Lin, *J. Chem. Phys.*, 2014, **141**, 104308.
5 D. Stone, M. Blitz, L. Daubney, T. Ingham and P. Seakins, *Phys. Chem. Chem. Phys.*, 2013, **15**, 19119.
6 H. Huang, B. Rotavera, A. J. Eskola and C. A. Taatjes, *J. Phys. Chem. Lett.*, 2013, **4**, 3824–3824.
7 B. Laszlo, M. J. Kurylo and R. E. Huie, *J. Phys. Chem.*, 1995, **99**, 11701–11707.
8 J. Carlos Gómez Martín, P. Spietz and J. P. Burrows, *J. Photochem. Photobiol. Chem.*, 2005, **176**, 15–38.
9 E. S. Foreman and C. Murray, *J. Phys. Chem. A*, 2015, **119**, 8981–8990.